Numerical Investigation of Western Boundary Current Intensification

Computational Fluid Dynamics Project

Andrea Combette

ENS — ENSL — Master SdM

January 30, 2025

Outline

Introduction

- Western boundary currents (e.g., Gulf Stream, Kuroshio) are key drivers of global ocean circulation.
- Phenomenon: Western Intensification.
- Pioneering theories by Stommel (1948) and Munk (1950).

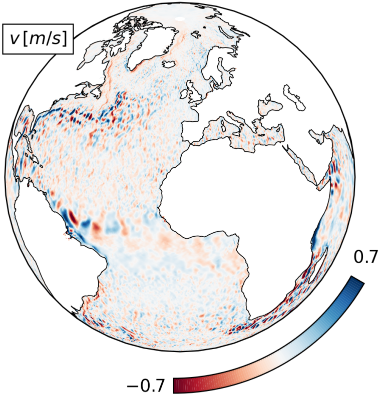

Figure – Atlantic Ocean surface meridional velocity.

Theoretical Background: Stommel and Munk Models

- Stommel (1948): Linear friction model.
- Munk (1950): Harmonic viscosity model.
- Governing equation:

$$\frac{\partial \zeta}{\partial t} + \mathcal{J}(\Psi, \zeta) + \beta \frac{\partial \Psi}{\partial x} = \nabla \times_z \boldsymbol{\tau} - r\Delta\Psi + A\Delta\zeta$$

- Key mechanisms:
  - *β-effect.*
  - *Wind stress forcing.*
  - *Frictional processes.*

Adimensionalization and Scaling

- Adimensionalization from a Sverdupian leading interior :

$$\beta \frac{\partial \Psi}{\partial x} = \nabla \times_z \boldsymbol{\tau}$$

- Key parameters:

$$\mathcal{R} = \frac{|\tau|}{\beta^2 L^3},$$
$$\epsilon_{\mathcal{S}} = \frac{r}{\beta L},$$
$$\epsilon_{\mathcal{M}} = \frac{A}{\beta L^3}$$

- This leads to :

$$\frac{\partial \zeta}{\partial t} + \mathcal{R}\mathcal{J}(\Psi, \zeta) + \frac{\partial \Psi}{\partial x} = \nabla \times_z \boldsymbol{\tau} - \epsilon_{\mathcal{S}} \Delta \Psi + \epsilon_{\mathcal{M}} \Delta \zeta$$

Linear System

- We consider the steady state of the system. We have :

$$\frac{\partial \Psi}{\partial x} = \nabla \times_z \boldsymbol{\tau} - \epsilon_{\mathcal{S}} \Delta \Psi + \epsilon_{\mathcal{M}} \Delta \zeta$$

- Considering in the stommel case ($\epsilon_{\mathcal{M}} = 0$) the matched boundary solution $\boldsymbol{\Psi}_{\mathcal{B}}$ and the matched interior solution $\boldsymbol{\Psi}_{\mathcal{I}}$ we have :

$$\begin{cases} \Psi_{\mathcal{B}} = -2\sin(y) e^{-\frac{x}{\epsilon_{\mathcal{S}}}} \\ \Psi_{\mathcal{I}} = (1+\cos(x))\sin(y) \end{cases}$$

- We now have the total solutions $\boldsymbol{\Psi} = \boldsymbol{\Psi}_{\mathcal{B}} + \boldsymbol{\Psi}_{\mathcal{I}}$:

$$\Psi = (1+\cos(x))\sin(y) - 2\sin(y) e^{-\frac{x}{\epsilon_{\mathcal{S}}}}$$

- We expect a boundary layer of typical size

$$\delta_{\mathcal{S}} \propto \epsilon_{\mathcal{S}} \quad | \quad \delta_{\mathcal{M}} \propto \epsilon_{\mathcal{M}}^{\frac{1}{3}}$$

Transport in the two models

- If we take the matching case

$$\epsilon_{\mathcal{S}} = \epsilon_{\mathcal{M}}^{\frac{1}{3}} = \epsilon$$

- We can find that the kinetic energy scaling follows :

$$\mathcal{K}_{\mathcal{S}} \propto \epsilon^{-1} \quad | \quad \mathcal{K}_{\mathcal{M}} \propto \epsilon^{-1}$$

  with $\mathcal{K}_{\mathcal{S}} < \mathcal{K}_{\mathcal{M}}$ leading to an higher transport in the Munk model for the same boundary size.

- Hence the two models can not unearth quantitative behavior on the western intensification

Non linear steady system

- We now consider the non-linear steady state of the system at small $\mathcal{R}$. We have :

$$\frac{\partial \Psi}{\partial x} + \mathcal{R}\mathcal{J}(\Psi, \zeta) = \nabla \times_z \boldsymbol{\tau} - \epsilon_{\mathcal{S}} \Delta \Psi + \epsilon_{\mathcal{M}} \Delta \zeta$$

- The idea is then to develop the stream function in power of $\mathcal{R}$:

$$\Psi = \Psi_0 + \mathcal{R}\Psi_1 + \dots$$

The zero-th order is the previous linear case and the first order unearthed :

$$\frac{\partial \Psi_1}{\partial x} + \epsilon_{\mathcal{S}} \Delta \Psi_1 = \mathcal{J}(\Psi_0, \zeta_0)$$

- This is the same equation as the linear case with the jacobian that plays the role of the wind stress, leading to :

$$\Psi = \Psi^{\mathcal{S}} - \frac{2\xi\mathcal{R}}{\epsilon_{\mathcal{S}}^2} \sin(2y) e^{\xi}$$

with $\xi = \frac{x}{\epsilon_{\mathcal{S}}}$.

$$\Psi = \Psi^{\mathcal{S}} - \frac{2\xi\mathcal{R}}{\epsilon_{\mathcal{S}}^2}\sin(2y)e^{\xi}$$

- This perturbated solution presents a poleward shift of the gyre with a concurrency near the boundary layer between the inertial and the viscous term :

$$\left|\frac{\Psi_1^{\mathcal{B}}}{\Psi_{\mathcal{B}}^{\mathcal{S}}}\right| = \frac{\mathcal{R}}{\epsilon_{\mathcal{S}}^2}, \quad x = \delta_{\mathcal{S}}$$

- At the top, contour plot of the linear stommel solution $\Psi_l^{\mathcal{S}}$, with $\epsilon_{\mathcal{S}} = 0.05$. At the bottom, the perturbed stommel solution at the bottom : $\Psi_{nl}^{\mathcal{S}}$ for $\epsilon_{\mathcal{S}} = 0.05$ and $\mathcal{R} = 0.005$.

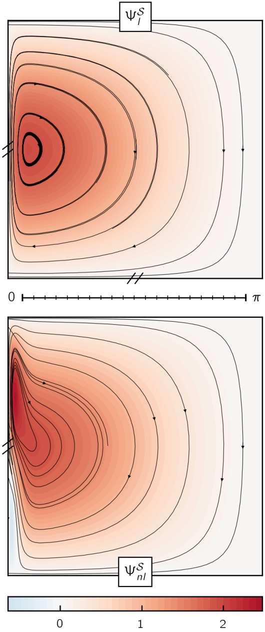

- At very high $\mathcal{R}$ the solution is fully inertial and that will lead to a famous type of flow : Fofonoff flow.
- For intermediate and high $\mathcal{R}$ numerical simulations are needed to understand the behavior of the system. since there is no simple analytical solution.

Numerical Implementation

- Finite difference discretization.

$$\Delta x = \Delta y = \frac{\pi}{N-1}$$

$$\partial_x \Psi = \frac{\Psi_{i+1,j} - \Psi_{i-1,j}}{2\Delta x}$$

- Temporal scheme: Leapfrog method.

$$\partial_t \Psi = \frac{\Psi^{n+1} - \Psi^{n-1}}{2\Delta t}$$

- Stability considerations:
  - *CFL, diffusive and drag conditions.*
- Laplacian and Jacobian operators:

$$\mathcal{L}\zeta_{ij} = \frac{\zeta_{i+1,j} + \zeta_{i-1,j} + \zeta_{i,j+1} + \zeta_{i,j-1} - 4\zeta_{ij}}{\Delta x^2}$$

$$\begin{aligned}\mathcal{J}_{ij}^n = & \left[(\Psi_{i+1,j+1}^n - \Psi_{i-1,j+1}^n)\zeta_{i,j+1}^n \right. \\ & \left. - (\Psi_{i+1,j-1}^n - \Psi_{i-1,j-1}^n)\zeta_{i,j-1}^n\right] \\ & - \left[(\Psi_{i+1,j+1}^n - \Psi_{i+1,j-1}^n)\zeta_{i+1,j}^n \right. \\ & \left. - (\Psi_{i-1,j+1}^n - \Psi_{i-1,j-1}^n)\zeta_{i-1,j}^n\right]\end{aligned}$$

Friction Stability

- If we consider the following discretized equation with a centered drag term :

$$\frac{\zeta_{ij}^{n+1} - \zeta_{ij}^{n+1}}{2\Delta t} + \mathcal{R}\mathcal{J}_{ij}^{n} = -\epsilon_{\mathcal{S}}\zeta_{ij}^{n} + \epsilon_{\mathcal{M}}\mathcal{L}\zeta_{ij}^{n} + \nabla \times_z \boldsymbol{\tau}$$

- growing instabilities can be observed, von-Neumann analysis leads to the consideration of the following harmonic wave functions :

$$\zeta = A\rho e^{ikx}, \quad \rho = e^{iwt}$$

If we restrict the study to the friction terms we get :

$$\rho^2 + 2\Delta t \epsilon_{\mathcal{M}}\rho - 1 = 0$$

This will lead to one unstable mode whatever the ρ we choose :

$$\rho = -\left[\Delta t \epsilon_{\mathcal{M}} + \sqrt{(\Delta t \epsilon_{\mathcal{M}})^2 + 1}\right] < -1$$

- One way to dress this issue is to consider the previous time step

$$\epsilon_{\mathcal{S}} \zeta_{ij}^{n} \rightarrow \epsilon_{\mathcal{S}} \zeta_{ij}^{n-1}$$

- it will leads to the following stability consideration:

$$\rho = \sqrt{1 - \epsilon_{\mathcal{M}} \Delta t} < 1$$

with $\epsilon_{\mathcal{M}} \Delta t \ll 1$ leading to :

$$\begin{aligned} \frac{\zeta_{ij}^{n+1} - \zeta_{ij}^{n+1}}{2\Delta t} + \mathcal{R} \mathcal{J}_{ij}^{n} = & - \epsilon_{\mathcal{S}} \zeta_{ij}^{n-1} \\ & + \epsilon_{\mathcal{M}} \mathcal{L} \zeta_{ij}^{n} \\ & + \nabla \times_z \boldsymbol{\tau} \end{aligned}$$

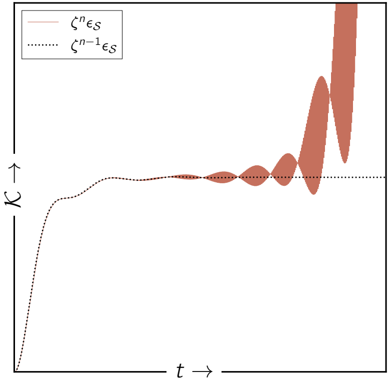

Figure – Kinetic Energy Overview of the instability induced by the central differences by using a centered friction term detailed in the previous section. This is not greatly noticeable for reasonable value of the $\epsilon_{\mathcal{S}}$ and $\mathcal{R}$

Overview

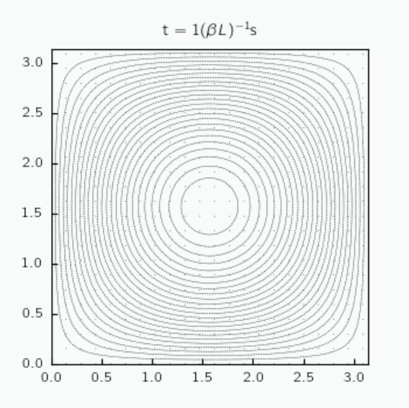

Figure – Temporal evolution of the fields for $\mathcal{R} = 8e - 3$ and $\epsilon_{\mathcal{S}} = 0.05$

Results: Boundary Layer Width

- Simulations were mase using free-slip BC
- Stommel and Munk models agree on scaling laws.
- Numerical results:
  - $\delta_{\mathcal{S}} \propto \epsilon_{\mathcal{S}}$.
  - $\delta_{\mathcal{M}} \propto \epsilon_{\mathcal{M}}^{1/3}$.

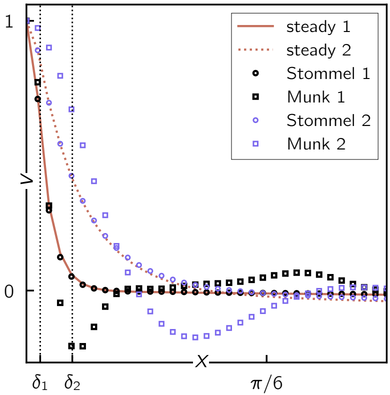

Figure – Normalized meridional velocity profiles. For different boundary layer size in black and in blue

Dynamics

- Difference of dynamic between the two model with trasncient aspect of the solutions for the Munk cases for free-slip boundary.
- Veronis attributed this transcient aspect to the no-slip BC. (shear flow)
- Bryan attributed this to Rossby free-wave in the bassin which maches the frequency.
- Why is this transcient aspect present in the Munk model and not in the Stommel case
- Kinetic Energy plot for the several boundary layer size in the matching case : $\epsilon_{\mathcal{M}}^{1/3} = \epsilon_{\mathcal{S}}$.

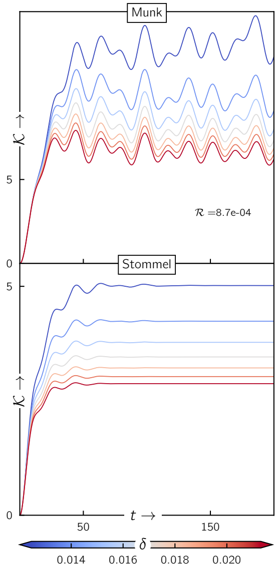

Dispersion Relations

- In this study we will get rid of the advection term hence we can use normal fourrier modes :

$$\Psi = \Psi_0 e^{i(\omega t - k_x x - k_y y)}$$

- this will leads in the Munk cases to the following dispersion :

$$\omega = \frac{k_x}{k_x^2 + k_y^2} + i\epsilon_{\mathcal{M}}(k_x^2 + k_y^2)$$

- Using the Stommel model this leads to :

$$\omega = \frac{k_x}{k_x^2 + k_y^2} + i\epsilon_{\mathcal{S}}$$

- The stommel model depicts a damping for all wavelength whereas it is *a priori* not the case in the Munk model.

Damping in the Munk Model

- As we explained it is possible for the Munk model to present a samping of the solutions but this is for large boundary layer width

- This allow dealing with higher non-linearity parameter but it should not be taken as a quantitative result for modeling the Gulf stream.

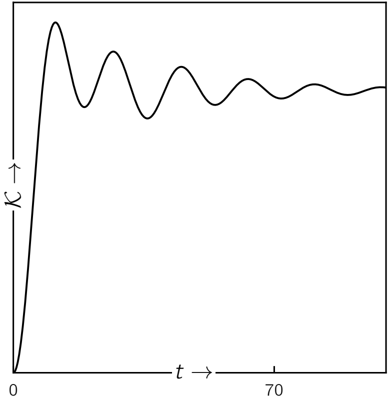

Figure – Stabilized Kinetic energy plot time evolution

Discussion: Instabilities in Munk and Stommel Models

- This unstable behavior was attributed by Munk to insufficient numerical precision for the damping dynamics in the boundary layer.

- We will see further that it is partially explaining the divergence , however it could have a physical origin with unstable growing mode at the nrthern boundary.

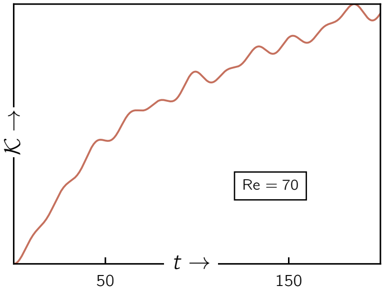

Figure – Energy time evolution for Re $= 70$, using $\epsilon_{\mathcal{M}} = 1.2e^{-5}$ and $\mathcal{R} = 9e^{-4}$

Divergent behavior study

- To study this unstable growing mode base on th two dispersion relation we have :

$$\omega_{\mathcal{M}} = \frac{k_x}{k_x^2 + k_y^2} + i\epsilon_{\mathcal{M}}(k_x^2 + k_y^2) \quad | \quad \omega_{\mathcal{S}} = \frac{k_x}{k_x^2 + k_y^2} + i\epsilon_{\mathcal{S}}$$

- we will suppose the following points
    - *at the beginning of the wind forcing the generated wave length are big and there is no boundary effect in the y direction*
    - *The west boundary layer will involve small scales and a disspiative boundary in the x-direction of small scale*
    - *the advection will mix the scales and will transfer small x scales to small y-scales*
    - *When the west boundary layer reach the north limit of the bassin, it will genreate dissipation in the y-direction .*

Illustration

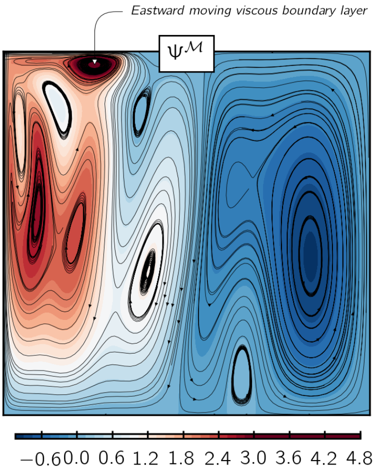

Figure – Contour plot of Ψ with streamlines in plain black, for a $\mathrm{Re} = 60$ at $t = 100(\beta L)^{-1}s$ with $\epsilon_{\mathcal{M}} = 1.5e^{-5}$. Small scales structures appear in both y and x direction with a strong eastward boundary layer flow at the northern boundary with a typical $k_x \sim 1 - 10$, corresponding to an unstable mode.

Munk case

- Using the previous dispersion relation for two typical case we unearth interesting behavior when considering small scales and dissipation in the y direction.
- Imaginary Frequency response contour plot over the k_x for two different k_y. *On the left :* we used a purely real $k_y = 1$. *On the right :* we used a complex $k_y = 30(1+i)$. The black plain line contour stands for the 0 level, hence it is the stability threshold of our model. The dashed contour line are negative contour.

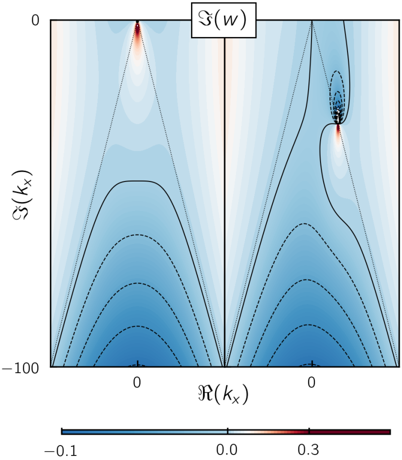

Munk case

- We recover the Bryan argument (the boundary layer should be sufficiently resolved
- However one thing that we can see is that, if the boundary layer reach the north boundary and that it is sufficiently small (allowing k_y to be important) this will lead to an unstable growing mode, that is purely physical.

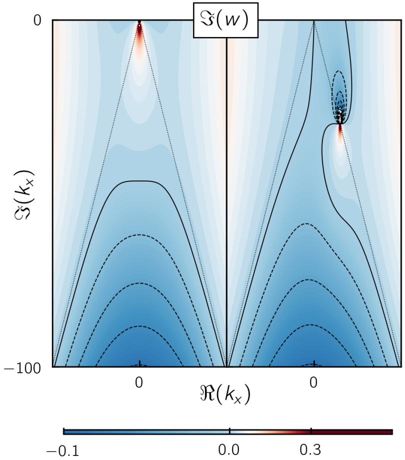

Stommel case

- The stommel case is interesting since it is damping equally all the frequency
- using this linear drag we lose the Bryan constraints
- there is some unstable mode but it is a restrict domain that is already damped and does not extend to pure propagating wave.

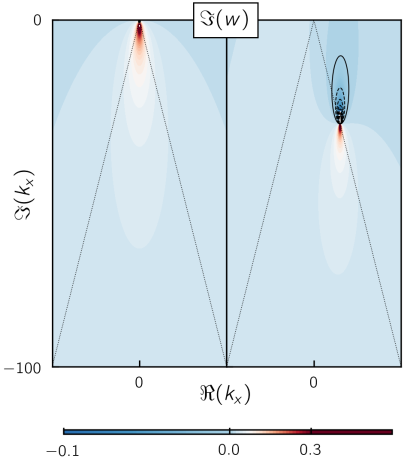

Checking the hypothesis

- small scales structures increasing with advection and the Re is quite obvious and is simply given by :

$$v\partial_x v \sim \epsilon_{\mathcal{M}} \partial_{xx} v$$

$$\frac{v^2}{\delta} \sim \epsilon_{\mathcal{M}} \frac{v}{\delta^2}$$

$$\delta \sim \frac{L}{\text{Re}}$$

- High-frequency modes emerge near the northern boundary layer.
- Power spectrum unearthed the same tendency with typical energy injection at the boundary layer scale.

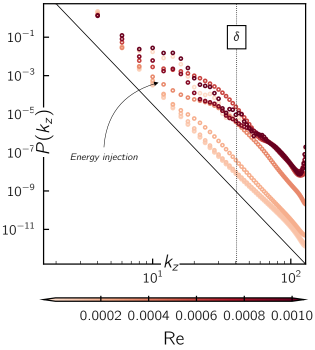

Figure – Spectral response for varying Reynolds numbers.

Checking the hypothesis

- small y scale structures increasing with time

- time dependent power spectrum for $Re = 60$, with $\epsilon_{\mathcal{M}} = 1.5e^{-5}$. The black plain line stand for a power law of $k_z^{-7.5}$

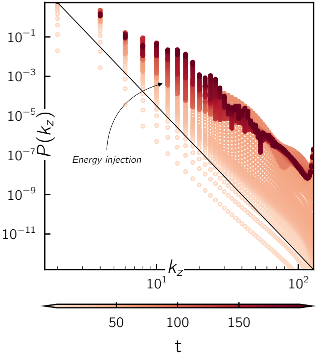

Checking the hypothesis

- Boundary layer northern intensification observed. leading to

$$\mathrm{Im}\, k_y \neq 0$$

- Western Boundary layer width evolution with the Reynolds number with $\epsilon_{\mathcal{M}} = 1.2e^{-5}$. The black dotted line stands for the theoritical width of the boundary layer.

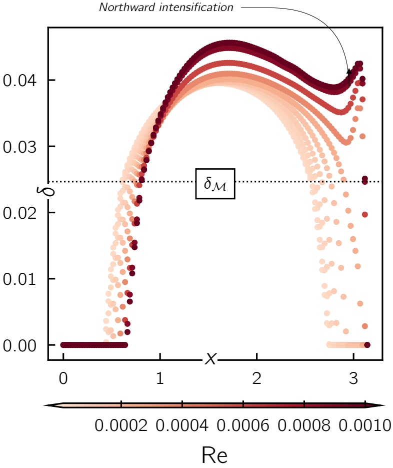

Low non linear regime

- our steady linear perturbation analysis corresponds exactly to the stommel model with a weak northward advection of the boundary layer

- Both stommel and Munk streamfunctions were average to get rid of transcient behavior. This shows a relatively higher transport in the Munk case.

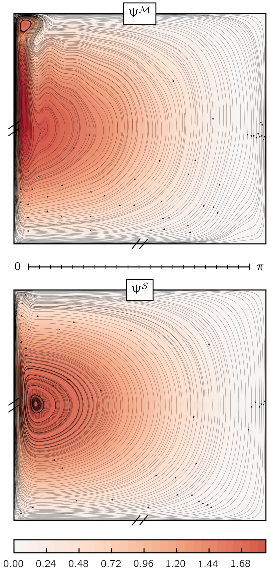

Scaling of the energy

- Munk model exhibits higher kinetic energy.
- Scaling laws:

$$\mathcal{K}_{\mathcal{S}} \propto \delta_{\mathcal{S}}^{-1},$$
$$\mathcal{K}_{\mathcal{M}} \propto \delta_{\mathcal{M}}^{-1}.$$

- Higher transport in Munk model.

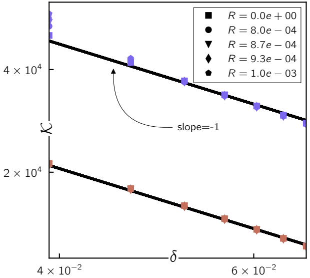

Figure – Kinetic energy scaling.

Discussion: Non-linear Regime

- Perturbative analysis:
  - *Northern intensification observed.*
  - *Inertial effects dominate at high Rossby numbers.*
- Emergence of Fofonoff solution in high non-linear regime without a south boundary layer ($y_0 = 0$).

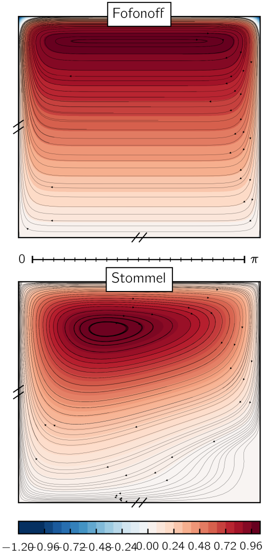

Real Wind Stress and Coastlines

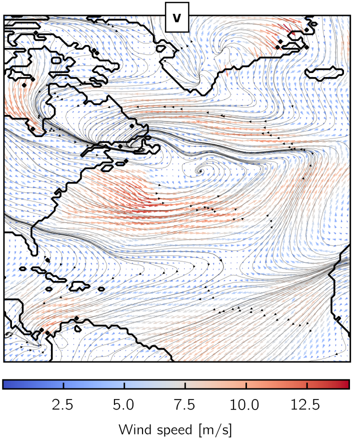

Figure – Global Atlantic velocity fields with streamlines from copernicus program

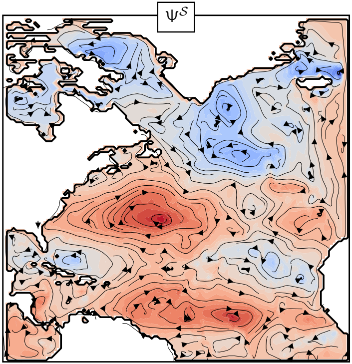

Figure – Global Atlantic solutions for stommel model with $\epsilon_{\mathcal{S}} = 0.02$ and $\mathcal{R} = 9e^{-4}$

Conclusion

- Numerical framework validated theoretical scaling laws.
- Stommel and Munk models provide complementary insights:
  - *Stommel: Simpler, stable.*
  - *Munk: higher transport (closer to real one) prone to instabilities.*